Received: 5 January 2023 | Revised: 8 May 2023 | Accepted: 18 May 2023

DOI: 10.1111/ter.12666

RESEARCH ARTICLE

Terra Nova WILEY

The control of collisional tectonics over valley morphology: the case of the largest glacier in the European Alps

Ferdinando Musso Piantelli[1,2] | Sandro Truttmann[1] | Marco Herwegh[1]

[1]Institute of Geological Sciences, University of Bern, Bern, Switzerland

[2]Swiss Geological Survey, Federal Office of Topography swisstopo, Bern, Switzerland

Correspondence
Ferdinando Musso Piantelli, Institute of Geological Sciences, University of Bern, Bern, Switzerland.
Email: ferdinando.musso@unibe.ch

Funding information
Federal Office of Topography of Switzerland (swisstopo; 570 300 4426 ARIWA 9101-01-Vertraege)

Abstract

Understanding how bedrock properties influence the valley-forming processes of Alpine landscapes is an outstanding challenge. A multi-methodological approach was used to uniformly quantify fault frequency, orientation, and rock hardness of crystalline basement rocks to evaluate their impact on the erosional processes that shaped the valley of the Aletsch Glacier, Switzerland. We show how variations in fault frequency and orientations, imposed by the inherited collisional framework of the area, controls the local erodibility of the valley, affecting both hillslopes and channel erosion processes. Our results highlight how tectonic preconditioning exerts a first-order control on the efficiency of erosion in the mountain chain, elucidating an integral link between deep-seated collisional dynamics and surface-based mountain shaping. Moreover, our results express the importance of a uniform, quantitative characterization of bedrock properties to comprehend the interaction and variability of erosional processes and hazards distributed within the valley systems.

1 | INTRODUCTION

In Alpine landscapes, most valleys form in a complex evolutionary sequence of widening and deepening controlled by channel incision and hillslope erosional processes (Harbor, 1992; MacGregor et al., 2000). Their efficiency is determined by the erosive power of the incising glacio-fluvial system and by the physical parameters of the bedrock. For example, unroofing of basement units in the core of mountain ranges is often associated with their lower erosional susceptibility to fluvial and glacial erosion (e.g., Carroll et al., 2006; Kühni & Pfiffner, 2001). However, such units are commonly affected by a large number of deformation structures (joints, faults, shear zones) induced during orogenesis (e.g. Molnar et al., 2007; Neely et al., 2019). Spatial variations in the occurrence of such deformation structures may lead to significant variability in relief production and erosional susceptibility (Patton et al., 2016; Steinemann et al., 2021; Whipple et al., 2000).

Geomorphological studies demonstrated that, under both glacial and fluvial settings, plucking and abrasion represent the two major channel incision erosional processes. While the first one dominates in densely fractured domains, the second one prevails in unfractured rock masses (Dühnforth et al., 2010; Sklar & Dietrich, 2001). Beside the incision processes, an increased fracture density also affects the stability of slopes resulting in hazardous landslide and rockfall events especially after glacial retreat (DiBiase et al., 2018; Moore et al., 2009).

So far, a direct link between a quantitative survey of fault distribution and valley morphology has received little attention. Yet understanding the spatial distribution and kinematics of fault patterns is a fundamental prerequisite not only for constraining valley-scale relief production and incision, but also for numerical models predicting valley evolution. In this study, a multi-methodological approach was followed to test the role of differential frequency distribution and orientation of faults in the valley morphology evolution of

the Aletsch Glacier (Central Switzerland); the largest glacier in the European Alps. This framework was used to evaluate landscape-scale valley morphology as a response to rock strength variation and structural variability to discuss implications for connections between collision geodynamics, landscape evolution, and natural hazards.

2 | GEOLOGICAL SETTING

The study area is located in the central Aar Massif, one of the External Crystalline Massifs of the European Alps, which recorded a long-lasting exhumation history. Differential uplift occurred along steep massif parallel fault and thrusts, consisting of mylonites, ultramylonites and prograde formation of cataclasites, fault gauges and breccias (see Appendix A and references therein). This resulted in both an N-S increasing metamorphic grade (up to the upper greenschist facies ~450°C; Herwegh et al., 2020; Nibourel et al., 2021) as well as a denser fault network. Given the both ductile and brittle nature of the structures, we refer to them in general as faults following the nomenclature of Sibson (1977). The exhumation accelerated in the last 1–2 million years due to the effect of glacial erosion (Fox et al., 2016; Glotzbach et al., 2010; Valla et al., 2011) and is still ongoing, as observed in differential rock uplift and seismic activity (e.g. Fäh et al., 2011; Schlatter et al., 2005). The valley object of this study is sculpted by the Great Aletsch Glacier and the Massa River (Figure 1a,b), with total length of ~30 km, of which ~22 km is occupied by the Aletsch Glacier. The bedrock units of the valley consist of migmatitic gneisses, granites, and granodiorites (Figure 1a). While the northern and southern part of the valley are underlain by migmatitic gneiss units (Figure 1a; Berger et al., 2017), fluid-altered migmatitic gneisses alternating with granite and granodiorite intrusion bodies occur in the central part (Figure 1a; Berger et al., 2017). The migmatitic gneiss units display a pre-Alpine foliation along which the faults localized (Wehrens et al., 2016).

In the North, three tributary glaciers converge at a triple junction named Konkordiaplatz and feed the main glacier (Figure 1a), coinciding with a large-scale ~350 m overdeepening (after Grab et al., 2021, Figure 1a). Further downstream the Aletsch glacier flows along a relatively straight NW-SW trending section before it abruptly changes its flow into NE–SW direction as induced by a series of ~30–50° turns, punctuated by a sequence of overdeepenings. The southern domains of the area are highly unstable as documented by several large-scale rock slope failures and rockfalls mostly related to recent glacial retreat (Glueer et al., 2019; Truttmann et al., 2021).

3 | METHODOLOGY

After a detailed field-based structural investigation (see Appendix A), a multi-methodological approach was employed to characterize and quantify the bedrock properties and hillslope morphology in a spatially uniform way over the entire study area.

(i) Remote sensing: The frequency distribution of the faults in the area was investigated remotely using a scan-line approach (Brooks & Allmendinger, 1996) continuously applied at the large-scale (1:2500), over the entire area, and at a more detailed scale (1:100) at four field locations (Figure 1a). The large-scale scan-lines consist of a sequence of individual segments oriented perpendicular to the main trend of the faults (Appendix B). Each linear feature detectable on orthophotos (raster resolution of 0.5×0.5 m) and hillshade maps (2×2 m raster resolution) being continuous for 100 m across the scan-line was sampled as a fault. The data were then projected onto a unified profile (Figure 1a, trace AA'), and plotted in a frequency histogram. The detailed-scale remote sensing frequency analysis was performed over UAV-based orthophotos and hillshade maps (raster resolution of 2.5×2.5 cm) at four different locations (Figure 1a and Table S2). At each location, the scan-lines were oriented perpendicular to the main trend of structures, and at locations 2, 3, and 4 also parallel to the main structural trend (Figure S6). This sampling strategy allowed obtaining the spatial pattern of faults, which in turn provided information about 2D block sizes available for channel and slope erosion processes.

(ii) Relief and slope analysis: To analyse the hillslope morphology of the valley both the hillslope angle and the relief were derived from 120 topographic valley transects perpendicular to the main valley axis with a spacing of 250 m. The average hillslope angle and relief were calculated on the right and left sides of the valley along each valley transect. (See Appendix B)

(iii) Schmidt hammer profiles: Field-based rock hardness analyses were performed with a Schmidt hammer (Classic 'N' type) along the scan-lines perpendicular to the structures at locations 1–4 (Figure 1a; Appendix B). The rebound values, together with the type of lithology and the presence of faults, were collected at regular 1 m sampling intervals on exposed rock surfaces parallel to the main foliation or related fault planes. The field locations were chosen in close vicinity to the glacier and within the Little Ice Age limit (Kelly et al., 2004) to ensure minimal weathering of the investigated outcrops.

4 | RESULTS

Both frequency and typology of faults are not uniform along the valley. According to the orientations and kinematics, three structural domains were characterized in the field (Figures 1c, 2; for details Appendix A). (i) A northern domain that displays gently South-dipping thrusts that cut steep reverse SW–NE striking faults (Figures 1c, 2a, b); (ii) a central and southern domain with steep reverse, SW–NE and SSW–NNE striking faults and SW–NE oriented strike-slip to oblique faults (Figures 1c, 2b,c); and (iii) a transition zone between the two aforementioned domains at Konkordiaplatz (TZ, Figure 1c, see Appendix A) where all the thrusts, reverse and strike-slip fault systems coexist. All the described structures are limited in width (dm–few m), but laterally very persistent and frequently traceable over several km.

The large-scale fault frequency analysis reveals variations from North to South (Figure 3a). From km 0 to 12.5 of the AA' transect

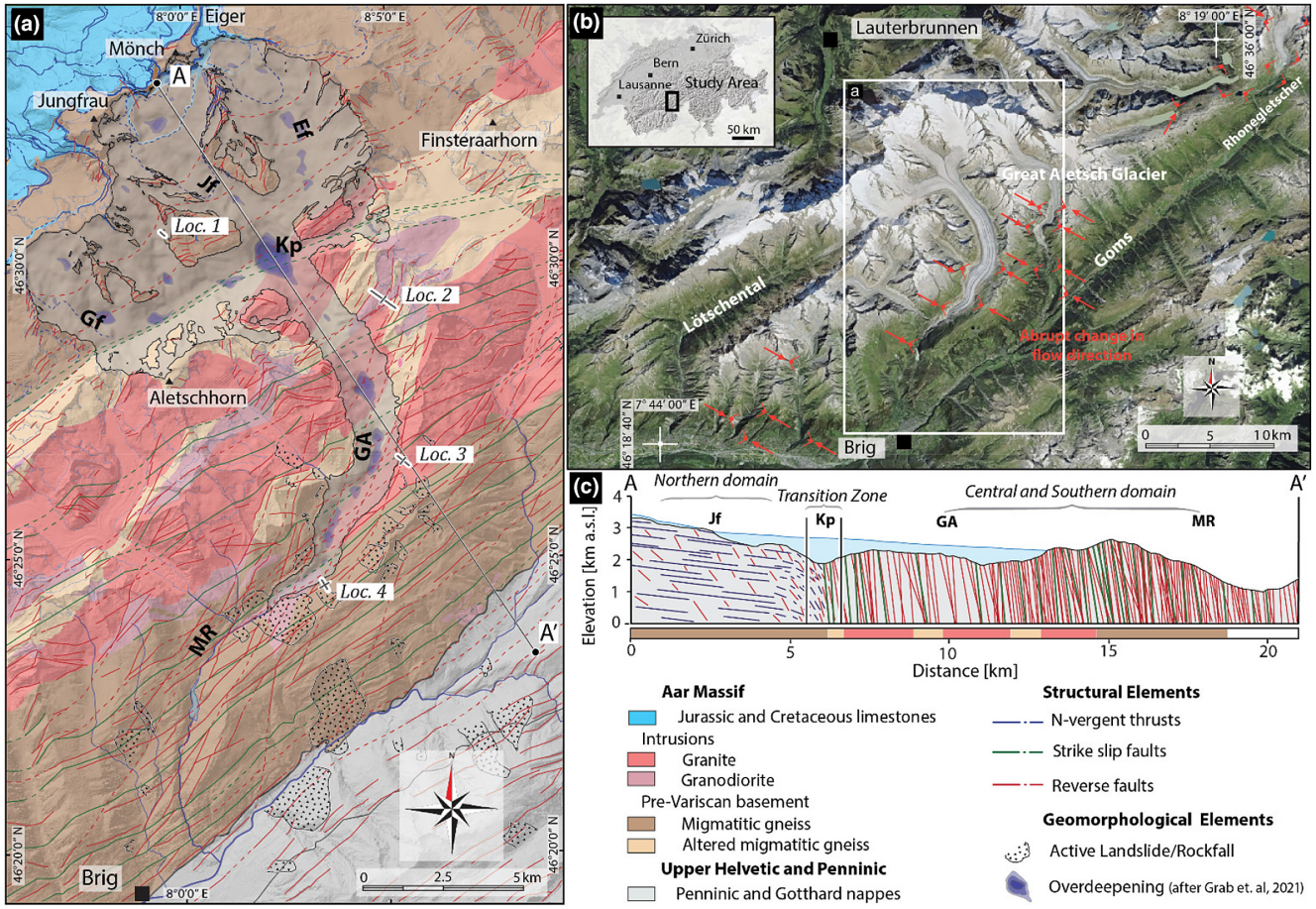

FIGURE 1 (a) Geological map of the investigated area. Purple colour-coded overdeepenings and hillshade of the glacier-bed topography after Grab et al., 2021. Active landslide/rockfall distribution from InSAR data (https://sitonline.vs.ch/dangers/dangers_geologiques/de/). Gf – Grosser Aletschfirn; Jf – Jungfraufirn; Ef – Ewigschneefäld; Kp – Konkordiaplatz; GA – Grosser Aletschgletscher; MR – Massa River. WGS84 coordinate system. (b) Large-scale overview (SWISSIMAGE, swisstopo) of the investigated area (white frame). The inset map shows the location within Switzerland. (c) Simplified geological section of the structures and lithologies in the study area. Section trace indicated in panel (a).

the faults reach a maximum spacing of 21.5 m. From km 12.5 to 22, the number of faults increases significantly, reaching a spacing of 14 m. These results correlate well with the detailed-scale fault frequency analysis (Figure 4). Indeed, transects at locations 1 and 2 reveal an average spacing, of the main structural trend, respectively of 3.24 m ± 1.90, and 3.42 m ± 2.94. This contrast significantly with transects at locations 3 and 4 that reveal an average spacing of 1.72 m ± 1.28, and 1.46 m ± 0.75. Also, the calculated 2D block sizes show larger blocks at location 2 (23.1 m^2) and smaller at locations 3 and 4, 7.5 and 7.4 m^2, respectively.

The relief and slope analyses (Figure 3b) show that the accumulation zone, which lies above 2500 m a.s.l., is weakly incised with gentle slope angles (20 to 30°) and a relief ranging between 700 to 900 m. Strong relief (800–1600 m) and steep slopes (20–38°) characterize the central sector, whereas the southern sector exhibit gentle hillslopes (>10 to 28°) and a strongly reduced relief (<1000 m).

The field-based Schmidt hammer analysis shows a bimodal distribution of the hardness measurements in all the investigated lithologies (Figure 3c). When not affected by a fault, all the lithologies range within similar hardness values (44 to 51 N/mm^3). However, in presence of a fault, the rocks' hardness drops systematically to significantly lower values of 29 to 34 N/mm^3.

5 | DISCUSSION AND CONCLUSIONS

The field-based Schmidt hammer investigations demonstrate that while lithological variations and rock foliation do not induce significant changes in rock hardness, the presence of faults considerably reduces the bulk rock hardness. Therefore the variations in orientation and frequency of faults, imposed by the geodynamic collisional framework of the Aar massif, are crucial in controlling: (i) bedrock erosion processes; (ii) valley axes orientation and morphology; and (iii) occurrence of hazardous mass movements in the Aletsch Glacier valley. As a function of those structural parameters, the valley morphology responds with a non-uniform susceptibility to bedrock erosion coupled in both the bedrock channel and hillslopes erosion processes.

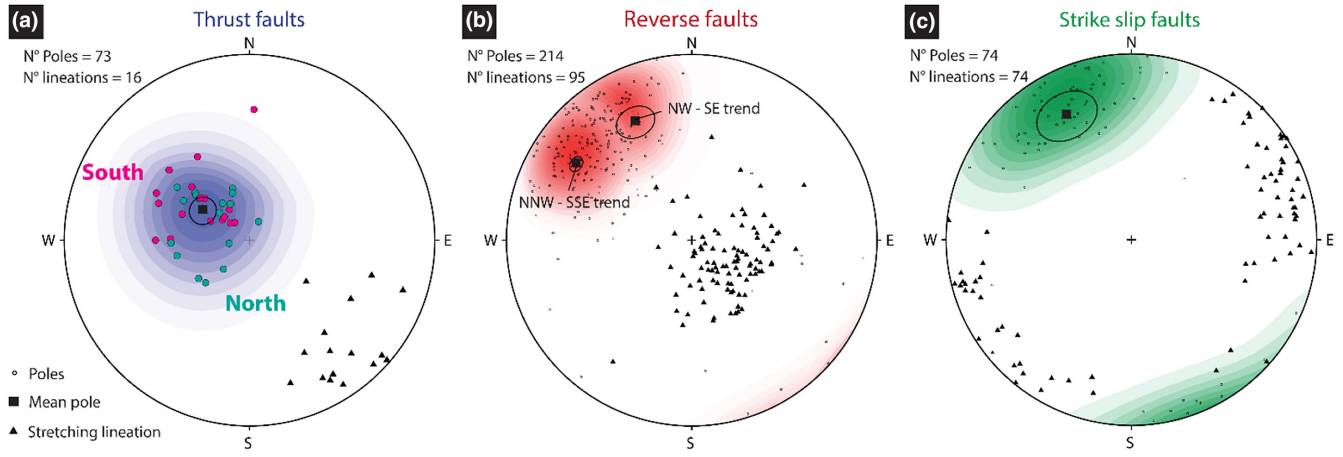

FIGURE 2 Structural field data (poles and mean poles for the fault planes and orientations of associated stretching lineation, lower hemisphere) of the fault structures in the basement units of the investigated area. (a) Stereoplot for the thrusts fault structures. As highlighted by the colour code of the poles, the fault planes increase progressively their dip angle from North to South. (b) Stereoplot for the reverse faults structures. In the plot, the two mean poles highlight the two different trends. (c) Dataset of the measurements of the strike slip faults.

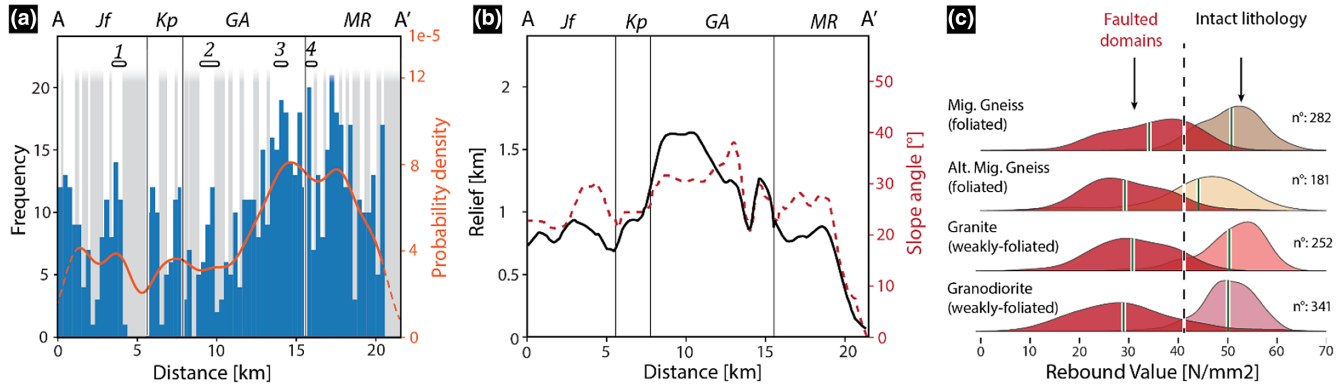

FIGURE 3 (a) Histogram (blue bars) and density curve (orange line) showing the large-scale frequency distribution of structures along the AA' profile (trace and abbreviations indicated in Figure 1a). Bin size of 300 m; the grey bars indicate no-data areas, that is areas covered by Quaternary deposits (see appendix A). (b) Moving averages of the relief (black line) and slope angle analysis (dashed red line) along the AA' profile (see Appendix A). (c) Ridgeline plot of the Schmidt hammer rebound values subdivided into the four lithological groups. The green bars indicate the mean rebound values of the intact and the faulted/sheared domains of each lithology.

5.1 | Dependency of channel incision processes on fault frequency and orientation

Fault frequency controls the erosional processes incising the valley channel as it defines the sizes of the blocks available for erosion (Whipple et al., 2000; Dühnforth et al., 2010). High-fault frequency bedrock, with mean fault spacing <2 m, is more prone to entrainment of blocks and therefore affected by high glacial and fluvial quarrying rates (Hallet, 1996; Patton et al., 2016; Steinemann et al., 2021). The enhanced quarrying rates lead to the generation of a large number of overdeepenings and bedrock riegels (Figure 5a,b). In low-fault frequency massive bedrock domains, with a mean fault spacing >2 m, quarrying becomes ineffective. Hence, the volumetrically less efficient abrasion process dominates generating relatively smooth bedrock sections (Figure 5a,b).

Fault orientation is another important factor since it determines the number of structural sets available for quarrying and the blocks' discharge direction. In the Transition Zone (Figure 5a) the three sets of faults render block discharge under quarrying very efficient, creating an ideal convergence point in the Konkordiaplatz overdeepening (>350 m; Grab et al., 2021). Furthermore, in the southern high-frequency fault domain, the SW–NE and SSW–NNE sets of structures establish the blocks' discharge direction under quarrying; presumably further exploiting an already formerly existing torrential system. Consequently, the observed sequences of overdeepenings and bedrock riegels evolved aligned with the two main fault

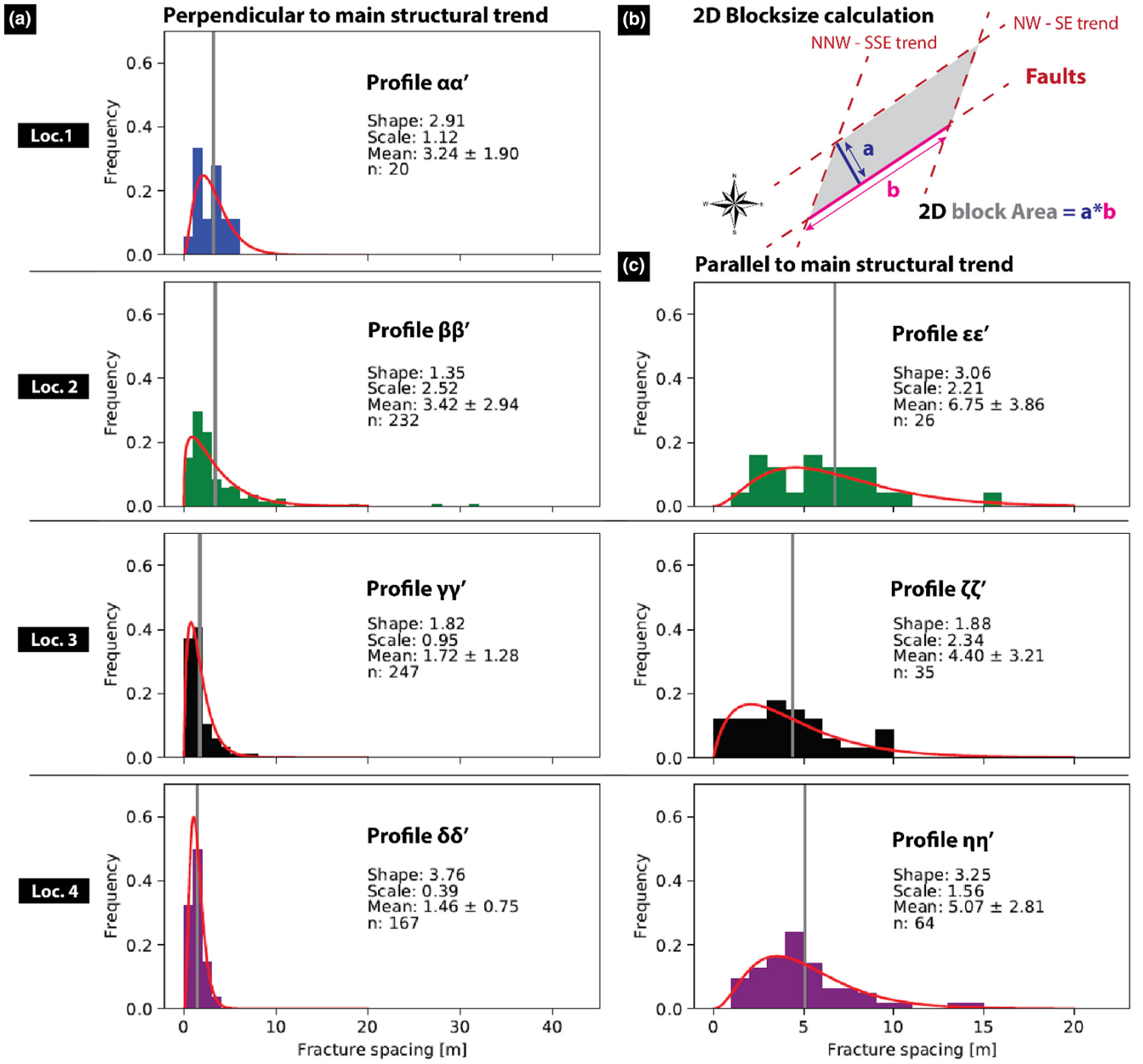

FIGURE 4 Probability density plots, fitted by a gamma distribution, of the fault spacing along each of the detailed scan lines perpendicular (a) and parallel (c) to the main structural trend. (b) Simplified sketch that shows the geometric calculation to derive the 2D block sizes at locations 2, 3, and 4. The block is sketched as a grey rhomboid bounded by the NNW – SSE and NW – SE trends of the fault structures present at the filed locations. (a) and (b) represent the mean fault spacing measured on the detailed scan-lines, respectively, oriented perpendicular and parallel to the main structural trend.

trends inducing the glacier's prominent turns in the flow direction (Figures 1a, 2b, 5b).

5.2 | Hillslope morphology dependency on fault frequency

The relief and slope analyses show a strong correlation between increasing fault frequency and decreasing bedrock hillslope-scale strength, expediting the hillslope erosion processes (e.g., DiBiase et al., 2018; Larsen & Montgomery, 2012). Indeed, high relief and steep slope angles characterize slopes in less faulted bedrock domains (Figure 5a,c) indicating high stability thresholds in terms of rockfalls and bedrock landslides. On the contrary, in highly faulted bedrock slopes (Figure 5a,d) low relief and gentle slope angles correspond to unstable slopes. This relation has important societal consequences in mountainous regions since these domains coincide with active hazardous large-scale bedrock landslides and rockfalls in the investigated area; that is, the currently active Moosfluh deep-seated bedrock landslide, one of the largest mass movements in the Alps (Glueer et al., 2019; Truttmann et al., 2021; Figures 5a,d).

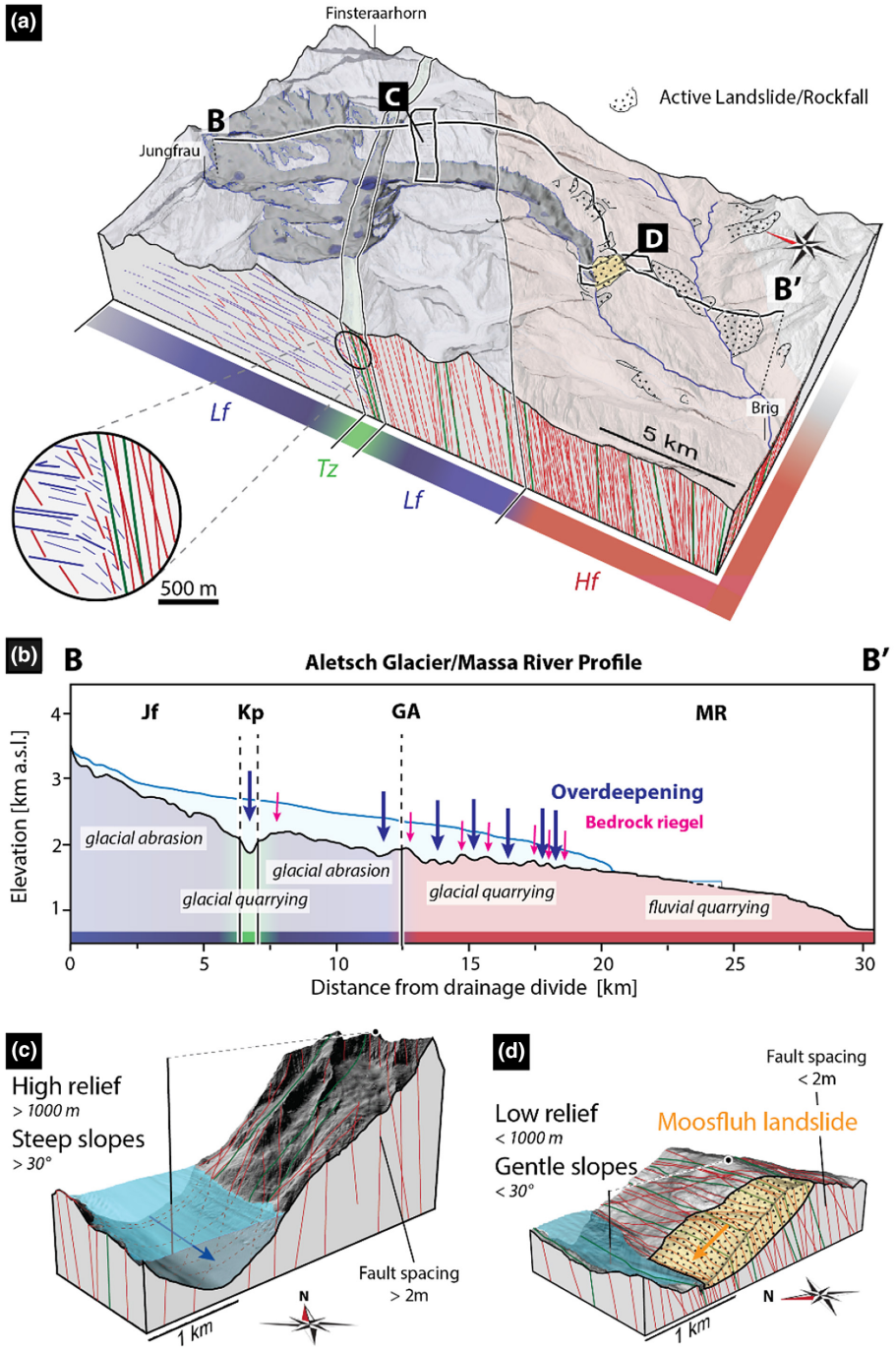

FIGURE 5 (a) 3D block model of the study area with subdivision into three domains based on the faults' frequency and kinematics. Low-frequency (Lf, blue), high-frequency (Hf, red), and transition zone (Tz, green) domains, respectively, with fault spacings of >2m, <2m and coexistence of reverse and strike-slip faults. (b) Longitudinal valley profile of the Aletsch Glacier and Massa River; profile trace visible in pane A. The Hf and Tz domains coincide with enhanced quarrying activity and the associated presence of overdeepenings and bedrock riegels. Instead, the Lf domains correspond to abrasion-dominated smooth bedrock sections. (c); 3D block model representing the hillslopes in Lf domain, box C in panel A. High slope stability granted by sparse fault spacing allows for the preservation of high relief and steep slope angles. (d) 3D block model representing the hillslopes in Hf domain, box D in pane A. Increased fault density reduces rock mass strength and triggers bedrock mass movements and rockfalls, that is, as expressed by the Moosfluh bedrock landslide. This results in a lowered relief and gentle slope angles.

5.3 | Alpine landscape evolution as a direct result of collisional tectonics?

From a geodynamic point of view, the fault structures evolved as a consequence of vertical tectonics during Alpine collision and exhumation (Herwegh et al., 2020 and references therein). Subsurface faults initiated at the crustal level therefore directly affect the efficiency of erosion in the mountain chain, elucidating an integral link between deep-seated collisional dynamics and surface-based mountain shaping. In other words, the efficiency of erosional

processes active in orogenic systems goes hand in hand with the inherited collisional tectonic architecture. Changes in the global climate system enhance then landscape disequilibrium and promote valley incision and relief development through both glacial and fluvial processes (Valla et al., 2011).

The discussed results express the importance of a uniform, quantitative characterization of fault distribution and orientation to comprehend the variability and interaction of erosional processes distributed within valley systems. Such quantification provides fundamental insights into long-term erosional patterns, essential for planning future hazards mitigation at the regional scale. This aspect is of particular societal relevance given the progressively retreating glaciers with consequently exposed oversteepened valley slopes resulting from climate change.

ACKNOWLEDGEMENTS

Our study was supported by the Federal Office of Topography of Switzerland (swisstopo; 570 300 4426 ARIWA 9101-01-Vertraege). We gratefully acknowledge Geotest AG for joint collaboration in the field, in particular H. Hartung-Hofmann, and S. Wettstein. T. Markmann is thanked for helping in the code development for the relief analysis. Open access funding provided by Universitat Bern.

DATA AVAILABILITY STATEMENT

The data that support the findings of this study are available from the corresponding author upon reasonable request.

REFERENCES

Berger, A., Mercolli, I., Herwegh, M., & Gnos, E. (2017). Geological ma of the Aar massif, Tavetsch and Gotthard Nappes, Federal Office of Topography Swisstopo, Scale 1: 100 000.

Brooks, B. A., & Allmendinger, R. W. (1996). Fault spacing in the El Teniente mine, Central Chile: Evidence for nonfractal fault geometry. *Journal of Geophysical Research*, *101*, 13633–13653. https://doi.org/10.1029/96JB00800

Carroll, A. R., Chetel, L. M., & Smith, M. E. (2006). Feast to famine: Sediment supply control on Laramide basin fi ll. *Geology*, *34*, 197–201. https://doi.org/10.1130/G22148.1

DiBiase, R. A., Rossi, M. W., & Neely, A. B. (2018). Fracture density and grain size controls on the relief structure of bedrock landscapes. *Geology*, *46*(5), 399–402.

Dühnforth, M., Anderson, R. S., Ward, D., & Stock, G. M. (2010). Bedrock fracture control of glacial erosion processes and rates. *Geology*, *38*(5), 423–426.

Fäh, D., Giardini, D., Kästli, P., Deichmann, N., Gisler, M., Schwarz-Zanetti, G., Alvarez-Rubio, S., Sellami, S., Edwards, B., Allmann, B., Bethmann, F., Wössner, J., Gassner-Stamm, G., Fritsche, S., & Eberhard, D. (2011). ECOS-09 Earthquake Catalogue of Switzerland Release 2011. Swiss Seismological Service ETH Zürich, Open-File Report 2011, SED/RISK/R/001/20110417.

Fox, M., Herman, F., Willett, S. D., & Schmid, S. M. (2016). The exhumation history of the European Alps inferred from linear inversion of thermochronometric data. *American Journal of Science*, *316*(6), 505–541.

Glotzbach, C., Reinecker, J., Danišík, M., Rahn, M., Frisch, W., & Spiegel, C. (2010). Thermal history of the central Gotthard and Aar massifs, European Alps: Evidence for steady state, long-term exhumation. *Journal of Geophysical Research: Earth Surface*, *115*(F3), 148–227. https://doi.org/10.1029/2009JF001304

Glueer, F., Loew, S., Manconi, A., & Aaron, J. (2019). From toppling to sliding: Progressive evolution of the Moosfluh landslide, Switzerland. *Journal of Geophysical Research: Earth Surface*, *124*(12), 2899–2919.

Grab, M., Mattea, E., Bauder, A., Huss, M., Rabenstein, L., Hodel, E., Linsbauer, A., Langhammer, L., Schmid, L., Church, G., Hellmann, S., Délèze, K., Schaer, P., Lathion, P., Farinotti, D., & Maurer, H. (2021). Ice thickness distribution of all Swiss glaciers based on extended ground-penetrating radar data and glaciological modeling. *Journal of Glaciology*, *67*(266), 1074–1092.

Hallet, B. (1996). Glacial quarrying: A simple theoretical model. *Annals of Glaciology*, *22*, 1–8.

Harbor, J. M. (1992). Numerical modeling of the development of U-shaped valleys by glacial erosion. *Geological Society of America Bulletin*, *104*(10), 1364–1375.

Herwegh, M., Berger, A., Glotzbach, C., Wangenheim, C., Mock, S., Wehrens, P., Baumberger, R., Egli, D., & Kissling, E. (2020). Late stages of continent-continent collision: Timing, kinematic evolution, and exhumation of the northern rim (Aar massif) of the Alps. *Earth-Science Reviews*, *200*, 102959. https://doi.org/10.1016/j.earscirev.2019.102959

Kelly, M. A., Kubik, P. W., Von Blanckenburg, F., & Schlüchter, C. (2004). Surface exposure dating of the great Aletsch glacier Egesen moraine system, western Swiss Alps, using the cosmogenic nuclide 10Be. *Journal of Quaternary Science: Published for the Quaternary Research Association*, *19*(5), 431–441.

Kühni, A., & Pfiffner, O. A. (2001). The relief of the Swiss Alps and adjacent areas and its relation to lithology and structure: Topographic analysis from a 250-m DEM. *Geomorphology*, *41*(4), 285–307.

Larsen, I. J., & Montgomery, D. R. (2012). Landslide erosion coupled to tectonics and river incision. *Nature Geoscience*, *5*(7), 468–473.

MacGregor, K. R., Anderson, R. S., Anderson, S. P., & Waddington, E. D. (2000). Numerical simulations of glacial-valley longitudinal profile evolution. *Geology*, *28*(11), 1031–1034.

Molnar, P., Anderson, R. S., & Anderson, S. P. (2007). Tectonics, fracturing of rock, and erosion. *Journal of Geophysical Research*, *112*, F03014. https://doi.org/10.1029/2005JF000433

Moore, J. R., Sanders, J. W., Dietrich, W. E., & Glaser, S. D. (2009). Influence of rock mass strength on the erosion rate of alpine cliffs. *Earth Surface Processes and Landforms*, *34*(10), 1339–1352.

Neely, A. B., DiBiase, R. A., Corbett, L. B., Bierman, P. R., & Caffee, M. W. (2019). Bedrock fracture density controls on hillslope erodibility in steep, rocky landscapes with patchy soil cover, southern California, USA. *Earth and Planetary Science Letters*, *522*, 186–197.

Nibourel, L., Berger, A., Egli, D., Heuberger, S., & Herwegh, M. (2021). Structural and thermal evolution of the eastern Aar massif: Insights from structural field work and Raman thermometry. *Swiss Journal of Geosciences*, *114*(1), 9.

Patton, H., Swift, D. A., Clark, C. D., Livingstone, S. J., & Cook, S. J. (2016). Distribution and characteristics of overdeepenings beneath the Greenland and Antarctic ice sheets: Implications for overdeepening origin and evolution. *Quaternary Science Reviews*, *148*, 128–145.

Schlatter, A., Schneider, D., Geiger, A., & Kahle, H. G. (2005). Recent vertical movements from precise levelling in the vicinity of the city of Basel, Switzerland. *International Journal of Earth Sciences*, *94*(4), 507–514.

Sibson, R. H. (1977). Fault rocks and fault mechanisms. *Journal of the Geological Society*, *133*(3), 191–213.

Sklar, L. S., & Dietrich, W. E. (2001). Sediment and rock strength controls on river incision into bedrock. *Geology*, *29*(12), 1087–1090.

Steinemann, O., Ivy-Ochs, S., Hippe, K., Christl, M., Haghipour, N., & Synal, H. A. (2021). Glacial erosion by the Trift glacier (Switzerland): Deciphering the development of riegels, rock basins and gorges. *Geomorphology*, *375*, 107533.

Truttmann, S., Herwegh, M., Schreurs, G., Ebert, A., & Hardmeier, S. (2021). The effect of pre-existing structures on the Moosfluh landslide and its lateral propagation (great Aletsch glacier, Switzerland). *Geomorphology*, *377*, 107530.

Valla, P. G., Shuster, D. L., & Van Der Beek, P. A. (2011). Significant increase in relief of the European Alps during mid-Pleistocene glaciations. *Nature Geoscience*, *4*(10), 688–692.

Wehrens, P., Berger, A., Peters, M., Spillmann, T., & Herwegh, M. (2016). Deformation at the frictional-viscous transition: Evidence for cycles of fluid-assisted embrittlement and ductile deformation in the granitoid crust. *Tectonophysics*, *693*, 66–84.

Whipple, K. X., Hancock, G. S., & Anderson, R. S. (2000). River incision into bedrock: Mechanics and the relative effi cacy of plucking, abrasion, and cavitation. *Geological Society of America Bulletin*, *112*, 490–503. https://doi.org/10.1130/0016-7606(2000)112<0490:RIIBMA>2.3.CO;2

SUPPORTING INFORMATION

Additional supporting information can be found online in the Supporting Information section at the end of this article.

Appendix A: Structural investigation

Appendix B: Methods: remote sensing, hillslope morphology analysis, and Schmidt hammer profiles

How to cite this article: Musso Piantelli, F., Truttmann, S., & Herwegh, M. (2023). The control of collisional tectonics over valley morphology: the case of the largest glacier in the European Alps. *Terra Nova*, *00*, 1–8. https://doi.org/10.1111/ter.12666